Supplemental Materials

Accurately predicting optical properties of rare-earth aluminate scintillators: influence of electron-hole correlations

Christopher N. Singh, Ghanshyam Pilania, Jan Barta, Blas Pedro Uberuaga, Xiang-Yang Liu

Materials Science and Technology Division
Los Alamos National Laboratory, Los Alamos, USA

(Dated: April 13, 2021)

Contents

1 Exploring exchange-correlation functionals in rare-earth perovskites **3**
1.1 Host electronic structure . . . 3
1.2 LuAP:Ce electronic structure . . . 5

2 Δ-SCF Manifold Occupations **9**
2.1 PBE+U Level . . . 9
2.2 HSE Level . . . 10

3 Simulation convergence criteria **10**
3.1 Dependence of total energy on basis set and momentum sampling . . . 10
3.2 Dependence of dielectric function on bands and kpoints . . . 12

4 Structural Analysis **13**

List of Figures

S1 **Schematic band diagram of activated $LuAlO_3$:Ce**. The left part of the figure is a cartoon diagram depicting possible locations of Ce^{3+} activator states. The right side of the figure shows the orthorombic (*Pnma*) $LuAlO_3$ unit cell (Figure by VESTA [1]). . . . 3
S2 **Contrasting gap size with functional.** Four functionals are shown, PBE [2], the mBJ parameterization by Koller et al [3], the mBJ parameterization for perovskites by Jishi et al [4], and the SCAN functional [5]. The Koller et al mBJ is the best approximation of E_g with only $\approx 1\%$ difference from experiment ($E_g = 8.44$ eV according to Kolobanov et al [6]). . . . 4
S3 **Contrasting Lu *f* state location with Hubbard U.** We find that increasing on-site interactions at the mean field level acts to rigidly shift the Lu *f* states down in energy, but does not change the fundamental gap. . . . 4
S4 **Effect of ionic relaxation at PBE+SO level.** This figure shows the effect of ionic relaxation on the activator states at the PBE level for multiple substitution sites. . . . 5
S5 **Effect of ionic relaxation at PBE+U level.** This figure shows the effect of ionic relaxation on the activator states at the PBE+U level for multiple substitution sites. . . . 6
S6 **Electronic structure with mBJ potential.** The figure contrasts the activated system with and without ionic relaxation at the PBE level, but using the mBJ functional for the final electronic structure. . . . 6
S7 **Contrasting large and small Ce concentration.** The figure contrasts native LuAP and doped LuAP:Ce. (a) shows the electronic structure as determined with the experimental lattice, and (b) shows the electronic structure with a fully relaxed structure. . . . 7
S8 **Electronic structure $LuAlO_3$:Ce 1.4%** This figure shows the effect of ionic relaxation on the activator states at the PBE+U level for multiple substitution sites. . . . 8
S9 **Effect of spin-orbit coupling and hybrid functionals.** Part (a) gives the effect of spin-orbit coupling within the PBE+U scheme. Part (b) contrasts the PBE+U and HSE functionals . . . 8

S10 **$LuAlO_3$:Ce convergence testing.** (a) The free energy with respect to basis set size (ENCUT). (b) The free energy with respect to minimum allowed k-point separation. We determine ENCUT = 480 eV and the k-spacing = 0.5 $Å^{-1}$ is sufficient. 11
S11 **$GdAlO_3$:Ce convergence testing.** (a) The free energy with respect to basis set size (ENCUT). (b) The free energy with respect to minimum allowed k-point separation. We determine ENCUT = 480 eV and the k-spacing = 0.5 $Å^{-1}$ is sufficient. 11
S12 **$YAlO_3$:Ce convergence testing.** (a) The free energy with respect to basis set size (ENCUT). (b) The free energy with respect to minimum allowed k-point separation. We determine ENCUT = 460 eV and the k-spacing = 0.5 $Å^{-1}$ is sufficient. 11
S13 **BSE k-point convergence testing in $YAlO_3$.** (a) The density of states with various k-meshes. (b) BSE vs DFT dielectric function on $2 \times 2 \times 2$ Γ centered k-mesh. (c) BSE vs DFT dielectric function on $3 \times 3 \times 3$ Γ centered k-mesh. (d) BSE vs DFT dielectric function on $4 \times 4 \times 4$ Γ centered k-mesh. 12
S14 **Experimental structural characterization** X-ray diffraction patterns of the $YAlO_3$:Ce and $GdAlO_3$:Ce samples prepared by quenching of the melt, compared to the ICDD PDF-2 database records of the relevant phases. 13

List of Tables

1 **PBE+U** Manifold occupations in ΔSCF (using VASP FERWE) 9
2 **HSE** Manifold occupations in ΔSCF (using VASP FERWE) 10

1. Exploring exchange-correlation functionals in rare-earth perovskites

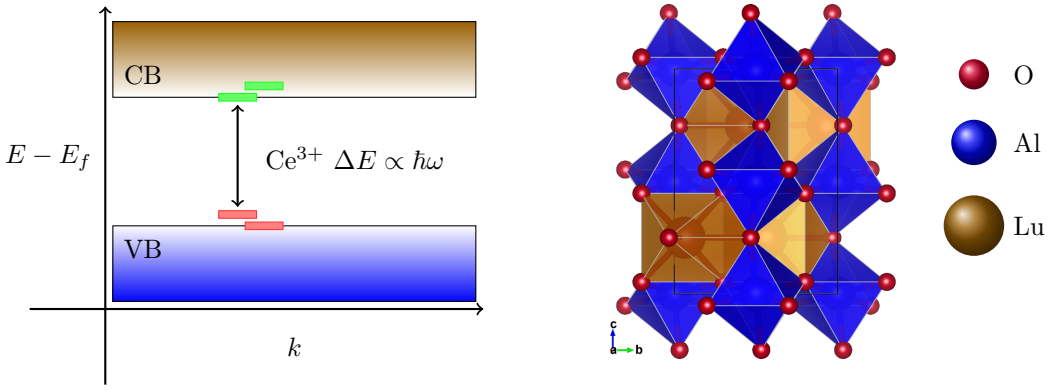

Figure S1: **Schematic band diagram of activated $LuAlO_3$:Ce**. The left part of the figure is a cartoon diagram depicting possible locations of Ce^{3+} activator states. The right side of the figure shows the orthorombic ($Pnma$) $LuAlO_3$ unit cell (Figure by VESTA [1]).

.

The location of activator states and size of the fundamental gap play an important role in the optical properties of rare-earth scintillators. Therefore, it is important to understand the effects of different exchange-correlation functionals on the fundamental gap and the location of the Ce states. Here we investigate the electronic structure of the host and activated systems with various functionals. The excited Ce state is Ce[Xe]$4f^0 5d^1$, sometimes denoted as $(Ce^{3+})^*$ and the ground state is Ce[Xe]$4f^1 5d^0$ (Ce^{3+}) [7]. A schematic of the electronic structure as well as the perovskite structure is given in figure S1. We use $LuAlO_3$ and $LuAlO_3$:Ce as a model system and extend the knowledge to the yttrium and gadolinium compounds.

1.1. Host electronic structure

In this section, we assume the experimental lattice parameters are sufficient to understand trends in the exchange-correlation functions. The effects of lattice relaxation in the activated systems will be shown in section 1.2. Figure S2 shows the density of states of $LuAlO_3$ with various functionals. The effect of spin-orbit coupling is also shown. In the host system, the mBJ type functionals have a better agreement with the experimental gap, but we will show later (in figure S6), that in the activated system, the mBJ functional does a poor job. Figure S2 also shows that the spin-orbit coupling does not change the gap size of the host appreciably, but it does split the degeneracy of the Lu f states.

Figure S3 shows how the Lu f states evolve with increasing Hubbard interaction U. In this figure we use the mean field construction developed by Anisimov et al [8, 9] and Liechtenstein et al [10]. The Hubbard U correction can be used to pin the location of the Lu f states to a location commensurate with photoemission data given by Dorenbos et al [11].

This data in figures S2 and S3 shows three things

1. The fundamental gap is underestimated by PBE and SCAN, but reasonable with mBJ
2. The spin-orbit coupling does not change the gap in the host, but it does split the Lu f states
3. The Hubbard U correction pins the Lu f states in the host system

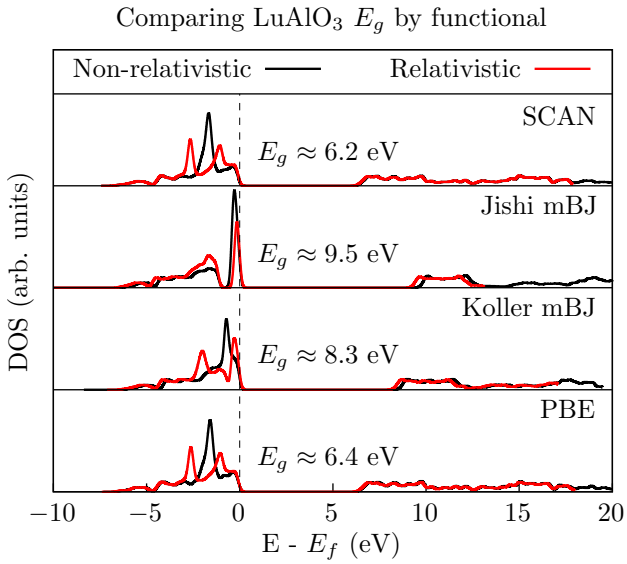

Figure S2: **Contrasting gap size with functional.** Four functionals are shown, PBE [2], the mBJ parameterization by Koller et al [3], the mBJ parameterization for perovskites by Jishi et al [4], and the SCAN functional [5]. The Koller et al mBJ is the best approximation of E_g with only $\approx 1\%$ difference from experiment ($E_g = 8.44$ eV according to Kolobanov et al [6]).

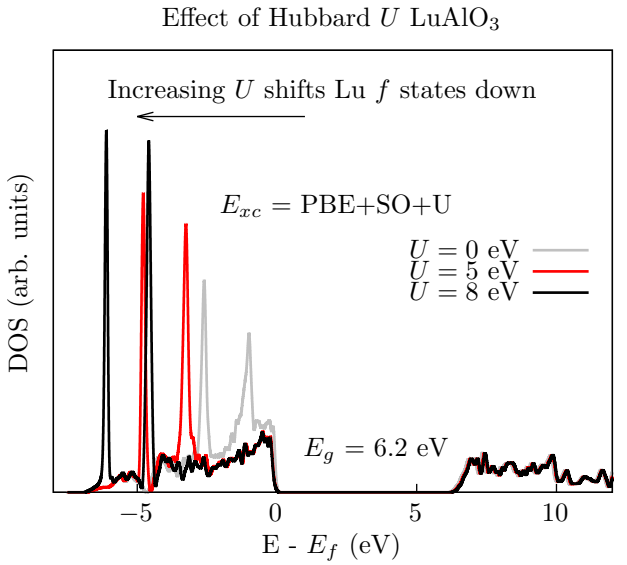

Figure S3: **Contrasting Lu f state location with Hubbard U.** We find that increasing on-site interactions at the mean field level acts to rigidly shift the Lu f states down in energy, but does not change the fundamental gap.

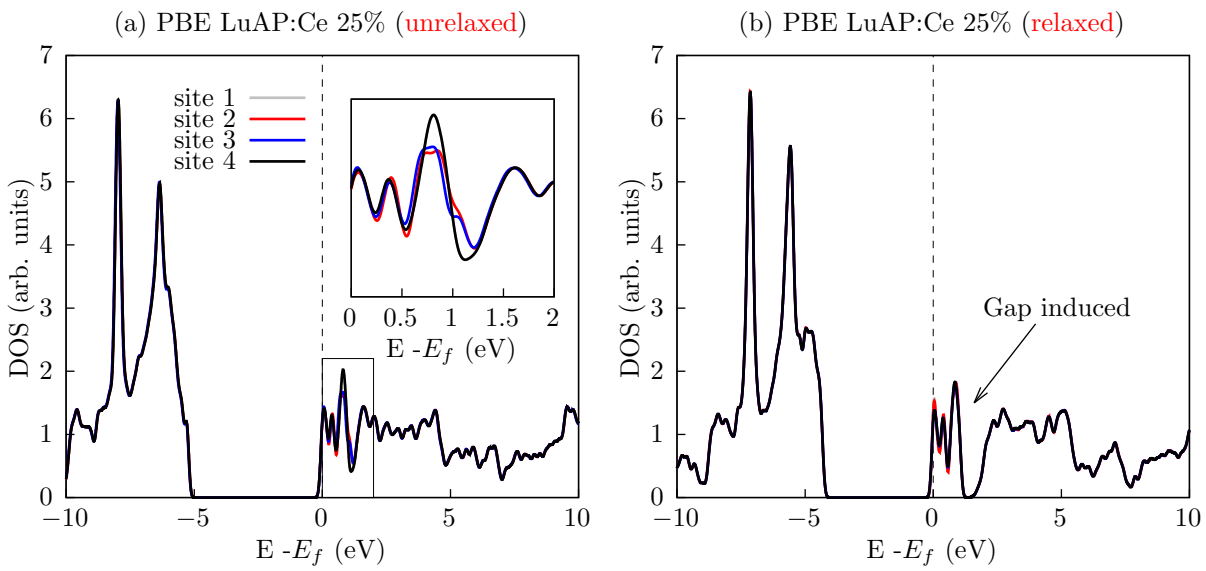

Figure S4: **Effect of ionic relaxation at PBE+SO level.** This figure shows the effect of ionic relaxation on the activator states at the PBE level for multiple substitution sites.

1.2. LuAP:Ce electronic structure

Figure S4 contrasts relaxed vs native (taken from experiment) electronic structure. We notice the metallic nature predicted by PBE. Because of the predicted metallic nature, we do not consider the GGA type functionals to be a good approximation to the Ce doped rare-earth perovskites. Part (a) suggests there are two inequivalent substitution sites in the 25% Ce cell, while part (b) shows that relaxation separates the Ce f states from the rest of the conduction bands.

Figure S5 shows the effects of ionic relaxation at the PBE+U level for $U = 4$ eV. We find that in both the relaxed (a) and unrelaxed (b) structures, each substitution site is degenerate, and that unlike PBE, PBE+U gapped the spectrum properly. The distance in energy between the valence band maximum (VBM), the Ce f state (single peak in the gap), and the conduction band minimum (CBM) is shown in the relaxed and un-relaxed case. We find the relaxation has several effects. It drives the occupied Ce f closer to the valence band, compresses the bandwidth of the primary valence states, and helps de-localize some of the primary conduction states. The changes to the valence and conduction bands are small. The shift in location of the Ce f is more pronounced, but as shown in the main text, its location can be tuned by the value of the Hubbard U parameter. In this sense, we make the approximation that the ionic relaxation is a net small change that can be mimicked with the proper U value.

Figure S6 shows the electronic structure of $LuAlO_3$:Ce with the mBJ functional (spin-orbit coupling is included). The effect of ionic relaxation is compared. We find the mBJ potential breaks many degeneracies between the Ce f and Ce d states. It also predicts a minimal spacing between the occupied Ce f state and unoccupied Ce states. This functional does a poor job because this electronic structure is not commensurate with the experimental emission wavelength.

Thus far we have been considering the 'alloy approximation', in that we have been using the unit cell and replacing one Lu atom by Ce (leading to 25% doping). Some experimental evidence, in the form of electron paramagnetic resonance (EPR) measurements by Buryi et al [12], suggests there is exchange coupling between neighboring Ce atoms. This indicates that the magnetic moment of the Ce ion should be considered as an interaction mediator in highly doped samples, therefore, we investigate the change in the electronic structure using larger supercells in figures S7 and S8.

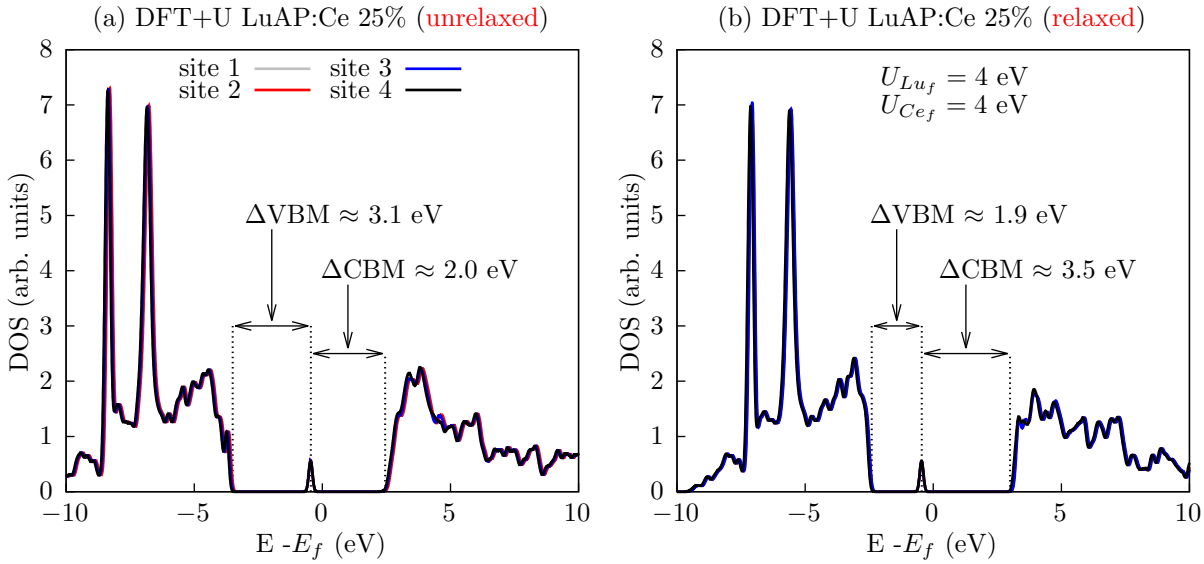

Figure S5: **Effect of ionic relaxation at PBE+U level.** This figure shows the effect of ionic relaxation on the activator states at the PBE+U level for multiple substitution sites.

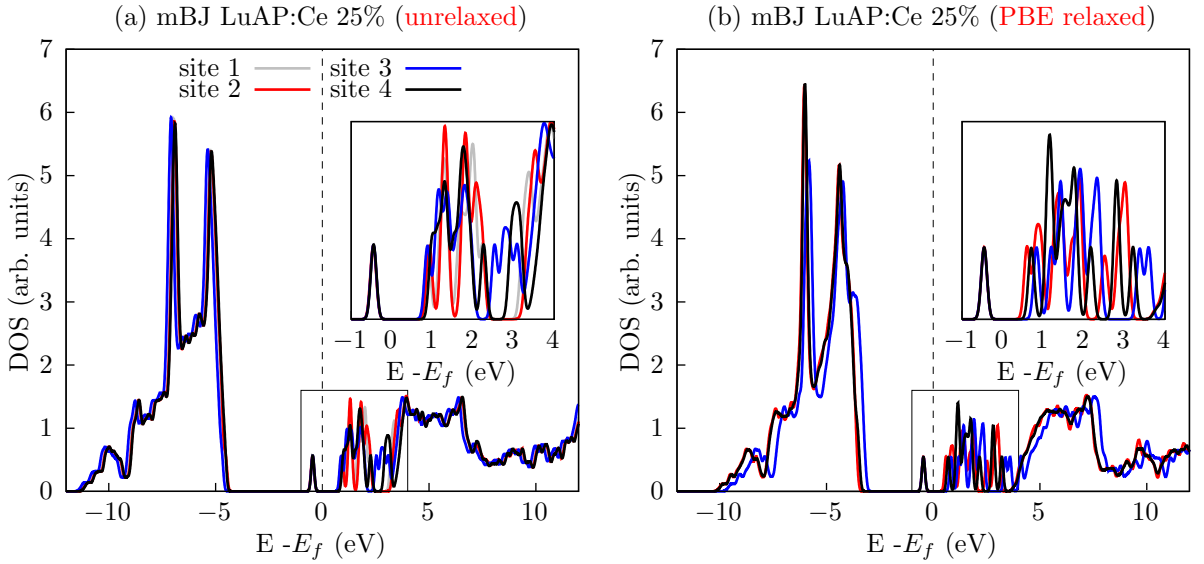

Figure S6: **Electronic structure with mBJ potential.** The figure contrasts the activated system with and without ionic relaxation at the PBE level, but using the mBJ functional for the final electronic structure.

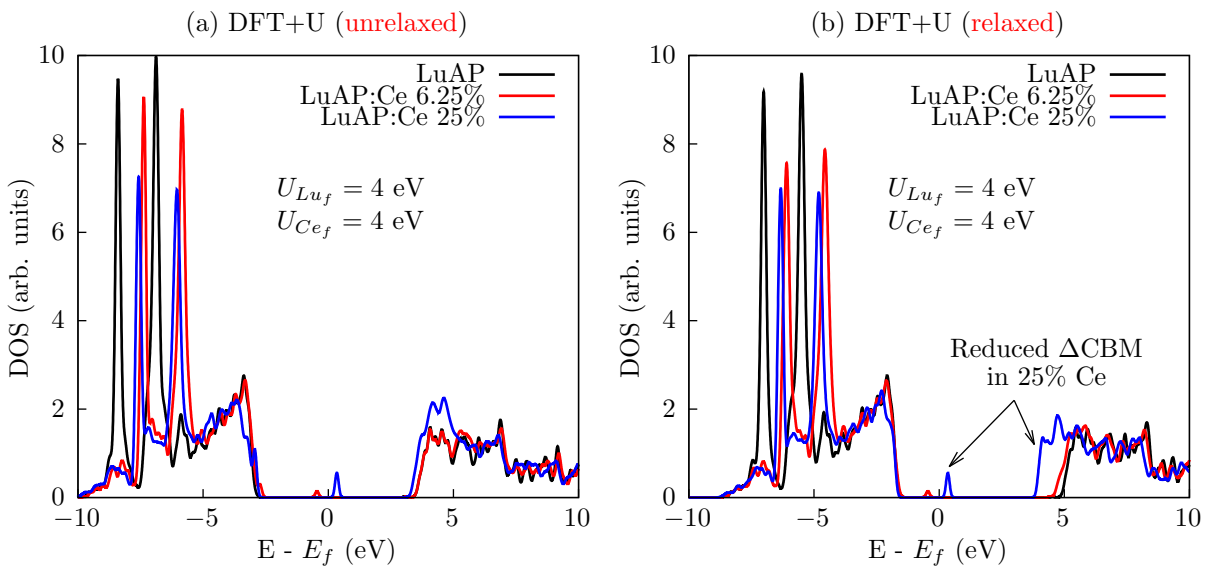

Figure S7: **Contrasting large and small Ce concentration.** The figure contrasts native LuAP and doped LuAP:Ce. (a) shows the electronic structure as determined with the experimental lattice, and (b) shows the electronic structure with a fully relaxed structure.

Figure S7 compares the density of states of the host, a 25% doped system, and a 6.25% doped system with and without ionic relaxation. We find that the ionic relaxation shifts the location of the activator states closer to the VBM, but also that the gap is ≈ 1 eV larger. When comparing this data to the Hubbard U dependence in the 25% doped sample, we see that increasing the Hubbard U value can give a result using the computationally simpler unit cell similar to the larger supercell. We use this data to choose a larger value of U such that the location of the Ce f state is closer to the VBM and the gap size is closer to experiment.

Figure S8 shows the projected density of states of $LuAlO_3$:Ce with 1.4% Ce (3x2x3) supercell. We find the fundamental gap does not change appreciably from the 25% doping case, however, an additional in-gap state is seen at the bottom of the conduction band. Its character is mostly s-like, suggesting it will have little impact on the optical properties. The cubic scaling of DFT with atom number means simulating the 1.4% doping condition is at least one to two orders of magnitude more expensive than the 25% unit cell. Given the minimal difference between the two, the 25% alloy approximation is valuable for the reduced computational cost.

Finally, we investigate the difference between the hybrid functionals and the PBE+U result, as well as the role of spin-orbit coupling in the cerium doped sample. Part (a) of figure S9 shows that inclusion of spin-orbit coupling drives delocalization of unoccupied Ce f states as well as deepening of the occupied singleton by nearly 4 eV. This is actually unexpected but not without rigorous theoretical evidence, for example, the relativistic nephelauxesis of Ce^{3+} is discussed by Petrov [13]. Part (b) of figure S9 shows that inclusion of exchange-correlation effects at the level of HSE tends to separate occupied Ce f level from valence band, and simultaneously increases the fundamental gap. The nearly 10-fold increase in computational expense however does not result in fundamentally different physics, i.e., the system is still gapped, the value is just different. In other words, the difference between the PBE and PBE+U result is much greater than the difference between the PBE+U and HSE result.

Based on investigating several functionals, the role of spin-orbit coupling, the role of ionic relaxation, and the role of the Hubbard U parameter, we take the unrelaxed system at the level of PBE+U as a reasonable approximation for the given computational burden.

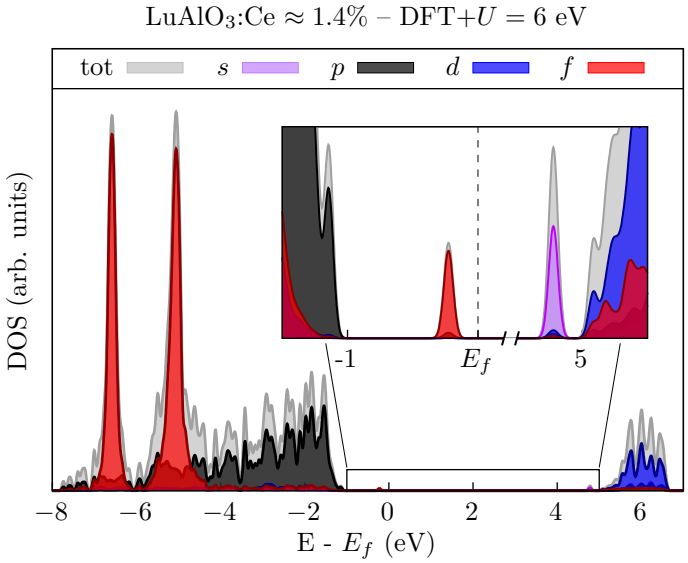

Figure S8: **Electronic structure $LuAlO_3$:Ce 1.4%** This figure shows the effect of ionic relaxation on the activator states at the PBE+U level for multiple substitution sites.

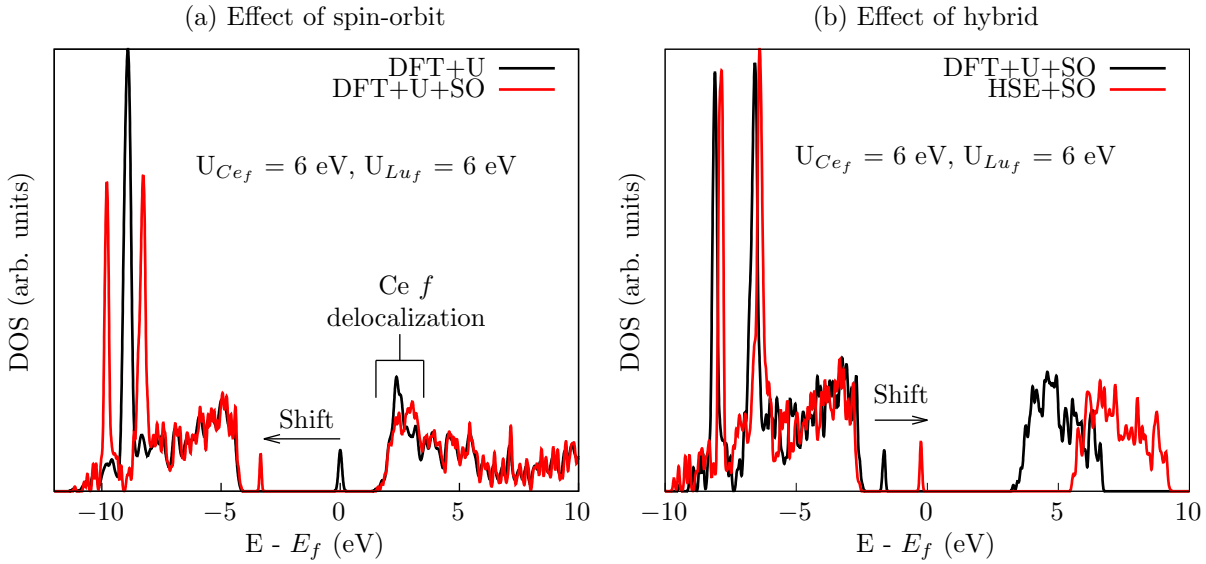

Figure S9: **Effect of spin-orbit coupling and hybrid functionals.** Part (a) gives the effect of spin-orbit coupling within the PBE+U scheme. Part (b) contrasts the PBE+U and HSE functionals

2. Δ-SCF Manifold Occupations

As mentioned in the main text, the manifold occupations are a main consideration in the Δ-SCF approach. This section tabulates the changes in orbital occupations in the Δ-SCF approach using PBE+U and HSE. It shows that the number of electrons transferred between the f and d manifolds in Ce is uncontrollable. In other words, fixing an occupation in the Kohn-Sham eigenspace does not correspond to the simple picture of single-electron $4f \rightarrow 5d$ transitions. Nevertheless, the dominant change is in Ce manifolds.

2.1. PBE+U Level

Table 1: **PBE+U** Manifold occupations in ΔSCF (using VASP FERWE)

(a) Ground state

ion	s	p	d	f	tot
Ce	1.977	5.795	**0.578**	**1.115**	9.464
Lu	2.206	6.138	0.862	14.275	23.481
Lu	2.205	6.134	0.850	14.271	23.459
Lu	2.211	6.134	0.881	14.275	23.501
Al	0.355	0.480	0.256	0.000	1.091
Al	0.354	0.479	0.256	0.000	1.089
Al	0.355	0.480	0.256	0.000	1.091
Al	0.354	0.479	0.256	0.000	1.089
O	1.521	3.507	0.000	0.000	5.028
O	1.520	3.508	0.000	0.000	5.028
O	1.520	3.509	0.000	0.000	5.029
O	1.524	3.529	0.000	0.000	5.053
O	1.520	3.508	0.000	0.000	5.028
O	1.521	3.507	0.000	0.000	5.028
O	1.524	3.529	0.000	0.000	5.053
O	1.520	3.509	0.000	0.000	5.029
O	1.525	3.522	0.000	0.000	5.047
O	1.521	3.544	0.000	0.000	5.066
O	1.522	3.549	0.000	0.000	5.071
O	1.524	3.493	0.000	0.000	5.017
tot	28.278	68.334	4.196	43.936	144.744

(b) Excited state

ion	s	p	d	f	tot
Ce	1.911	5.500	**0.828**	**0.471**	8.710
Lu	2.208	6.137	0.895	14.272	23.512
Lu	2.208	6.132	0.871	14.268	23.480
Lu	2.211	6.130	0.943	14.270	23.554
Al	0.356	0.480	0.257	0.000	1.093
Al	0.356	0.479	0.256	0.000	1.092
Al	0.356	0.480	0.257	0.000	1.093
Al	0.356	0.479	0.256	0.000	1.091
O	1.525	3.503	0.000	0.000	5.028
O	1.522	3.505	0.000	0.000	5.028
O	1.522	3.506	0.000	0.000	5.028
O	1.525	3.527	0.000	0.000	5.053
O	1.522	3.506	0.000	0.000	5.028
O	1.525	3.503	0.000	0.000	5.028
O	1.525	3.527	0.000	0.000	5.053
O	1.522	3.506	0.000	0.000	5.028
O	1.526	3.520	0.000	0.000	5.046
O	1.523	3.542	0.000	0.000	5.065
O	1.523	3.547	0.000	0.000	5.070
O	1.527	3.485	0.000	0.000	5.012
tot	28.251	67.997	4.563	43.281	144.092

Table 1 collects the orbital occupations in the ground and excited states of $LuAlO_3$:Ce using Δ-SCF and PBE+U scheme. We find that at the PBE+U level, significant electron density is transferred out of the Ce f state. Some of this density is picked up by the Ce d state, but some of it is passed into the interstitial because the total Ce occupation is reduced.

2.2. HSE Level

Table 2: **HSE** Manifold occupations in ΔSCF (using VASP FERWE)

(a) Ground state

ion	s	p	d	f	tot
Ce	2.100	5.821	**0.627**	**1.190**	9.738
Lu	2.175	6.147	0.795	14.179	23.296
Lu	2.174	6.143	0.783	14.176	23.276
Lu	2.181	6.144	0.814	14.179	23.318
Al	0.355	0.394	0.000	0.000	0.750
Al	0.354	0.394	0.000	0.000	0.748
Al	0.355	0.394	0.000	0.000	0.749
Al	0.354	0.393	0.000	0.000	0.748
O	1.560	3.599	0.000	0.000	5.159
O	1.558	3.603	0.000	0.000	5.161
O	1.558	3.602	0.000	0.000	5.160
O	1.563	3.620	0.000	0.000	5.183
O	1.558	3.603	0.000	0.000	5.161
O	1.560	3.599	0.000	0.000	5.158
O	1.563	3.621	0.000	0.000	5.184
O	1.558	3.602	0.000	0.000	5.160
O	1.564	3.613	0.000	0.000	5.177
O	1.563	3.641	0.000	0.000	5.203
O	1.564	3.645	0.000	0.000	5.209
O	1.561	3.584	0.000	0.000	5.145
tot	28.778	69.160	3.019	43.725	144.682

(b) Excited state

ion	s	p	d	f	tot
Ce	2.039	5.823	**0.785**	**0.774**	9.421
Lu	2.185	6.146	0.820	14.177	23.328
Lu	2.185	6.142	0.794	14.175	23.297
Lu	2.189	6.142	0.859	14.177	23.366
Al	0.356	0.394	0.000	0.000	0.750
Al	0.356	0.393	0.000	0.000	0.749
Al	0.356	0.394	0.000	0.000	0.750
Al	0.356	0.393	0.000	0.000	0.749
O	1.561	3.597	0.000	0.000	5.158
O	1.561	3.600	0.000	0.000	5.161
O	1.560	3.599	0.000	0.000	5.158
O	1.564	3.620	0.000	0.000	5.184
O	1.561	3.600	0.000	0.000	5.161
O	1.561	3.596	0.000	0.000	5.158
O	1.564	3.619	0.000	0.000	5.183
O	1.560	3.599	0.000	0.000	5.158
O	1.565	3.611	0.000	0.000	5.176
O	1.564	3.639	0.000	0.000	5.202
O	1.564	3.643	0.000	0.000	5.208
O	1.562	3.579	0.000	0.000	5.142
tot	28.767	69.130	3.258	43.303	144.458

Table 2 collects the orbital occupations in the ground and excited states of $LuAlO_3$:Ce using Δ-SCF and HSE functional. Much like the PBE+U result, at the HSE level, significant electron density is transferred out of the Ce f state, however, there is less transferred using HSE. Additionally, less electron density is transferred out of the Ce manifold entirely. We suspect this is because the improved treatment of exchange interactions in the HSE approach better account for the electron-hole attractive interaction and act to retain density within the Ce manifolds.

3. Simulation convergence criteria

3.1. Dependence of total energy on basis set and momentum sampling

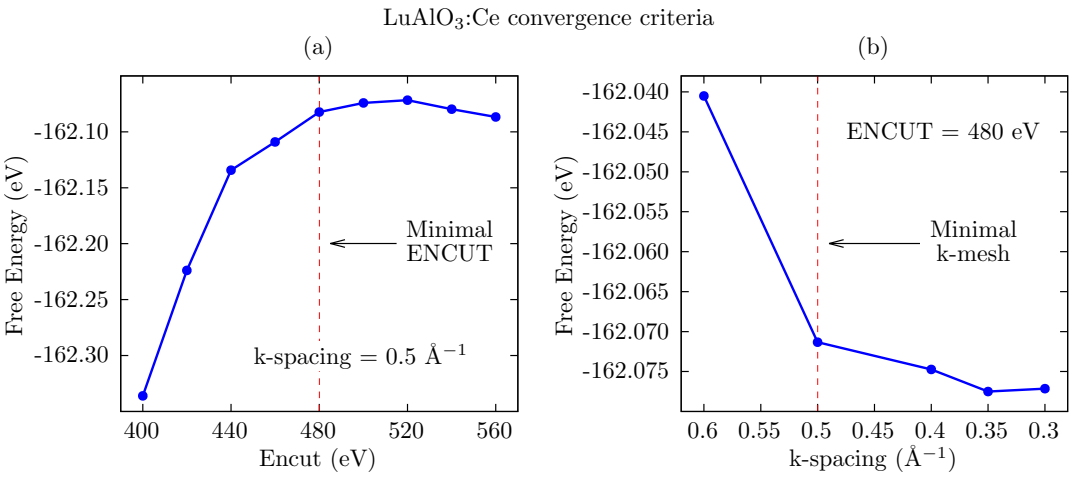

Figure S10: **$LuAlO_3$:Ce convergence testing.** (a) The free energy with respect to basis set size (ENCUT). (b) The free energy with respect to minimum allowed k-point separation. We determine ENCUT = 480 eV and the k-spacing = 0.5 $Å^{-1}$ is sufficient.

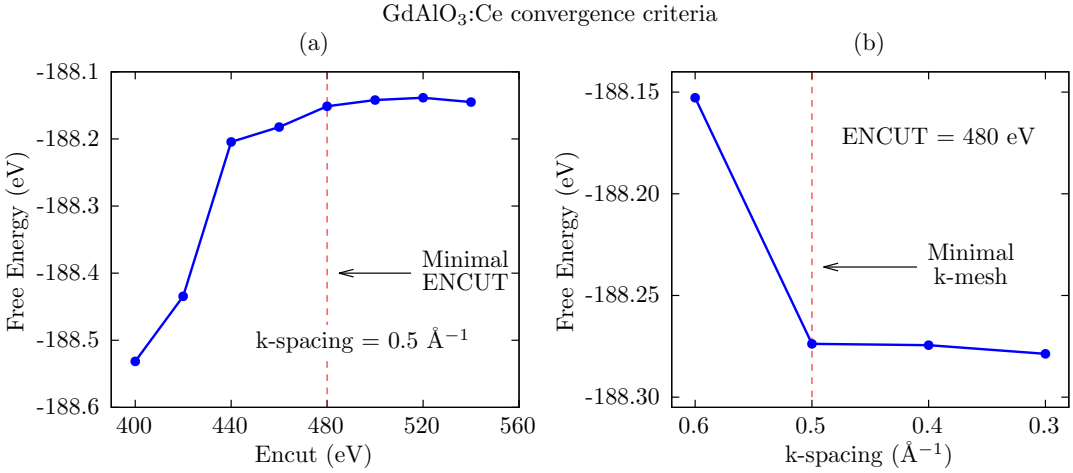

Figure S11: **$GdAlO_3$:Ce convergence testing.** (a) The free energy with respect to basis set size (ENCUT). (b) The free energy with respect to minimum allowed k-point separation. We determine ENCUT = 480 eV and the k-spacing = 0.5 $Å^{-1}$ is sufficient.

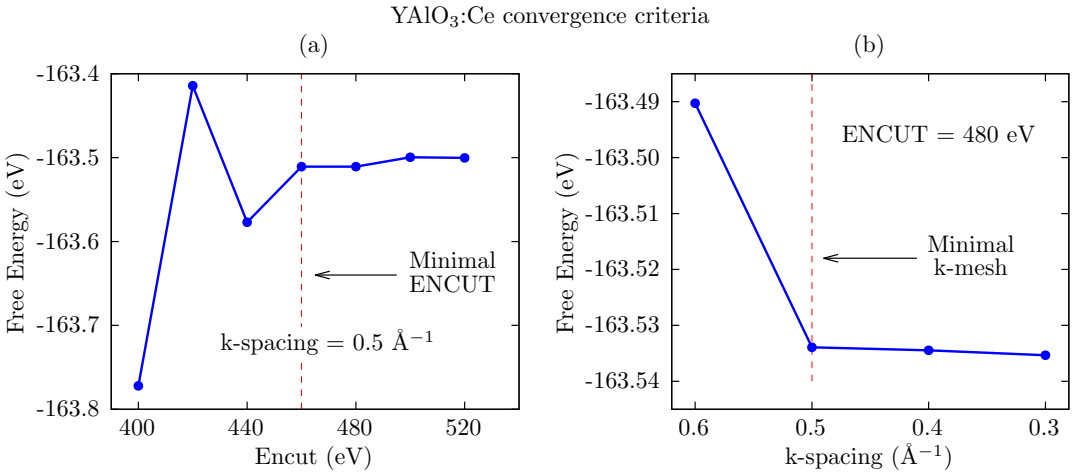

Figure S12: **$YAlO_3$:Ce convergence testing.** (a) The free energy with respect to basis set size (ENCUT). (b) The free energy with respect to minimum allowed k-point separation. We determine ENCUT = 460 eV and the k-spacing = 0.5 $Å^{-1}$ is sufficient.

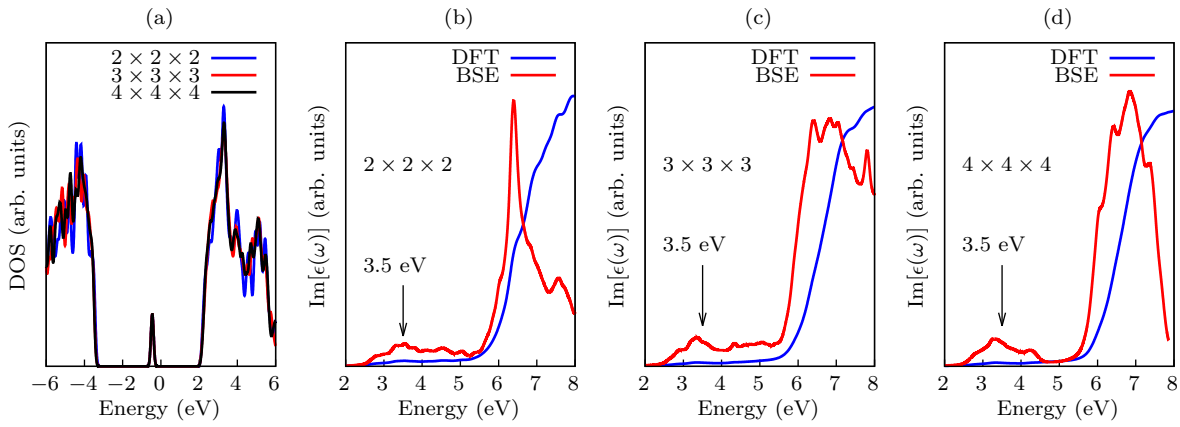

Figure S13: **BSE k-point convergence testing in $YAlO_3$.** (a) The density of states with various k-meshes. (b) BSE vs DFT dielectric function on $2 \times 2 \times 2$ Γ centered k-mesh. (c) BSE vs DFT dielectric function on $3 \times 3 \times 3$ Γ centered k-mesh. (d) BSE vs DFT dielectric function on $4 \times 4 \times 4$ Γ centered k-mesh.

3.2. Dependence of dielectric function on bands and kpoints

This section looks at the convergence of the dielectric functions with respect to calculation parameters. In general, we find that the detail nature of the simulation is sensitive to many parameters. However, the general features are not that sensitive, and are in line with the primary conclusion that electron correlations play a significant role. For example, in part (a) of figure S13, we see that the density of states can change only slightly with different k-meshes. The critical feature – the location of the mid-gap Ce f level – is not sensitive to the k-mesh. In fact, smearing and integration techniques can lead to larger differences in the density of states than the k-meshes are making here. The remaining parts of figure S13, part (b), (c), and (d) give a comparison of the DFT and BSE dielectric functions for various k-meshes. Independent of the k-mesh, we find a low energy peak appearing near 3.5 eV that is mostly absent in the DFT result. At low momentum space resolution ($2 \times 2 \times 2$), the peak is fairly broad. However, with increasing momentum space resolution, this peak becomes sharper and sharper. Going beyond a $4 \times 4 \times 4$ mesh starts to become too expensive for the information gained, because, although an approximately 0.1 eV movement is observed going from $2 \times 2 \times 2$ to $4 \times 4 \times 4$, the salient feature here is that a single particle DFT prediction would be multiple eV displaced. It is for this reason that although the fine structure may change with k-point sampling, we conclude that relatively few kpoints are needed to make significantly improved predictions compared to standard DFT.

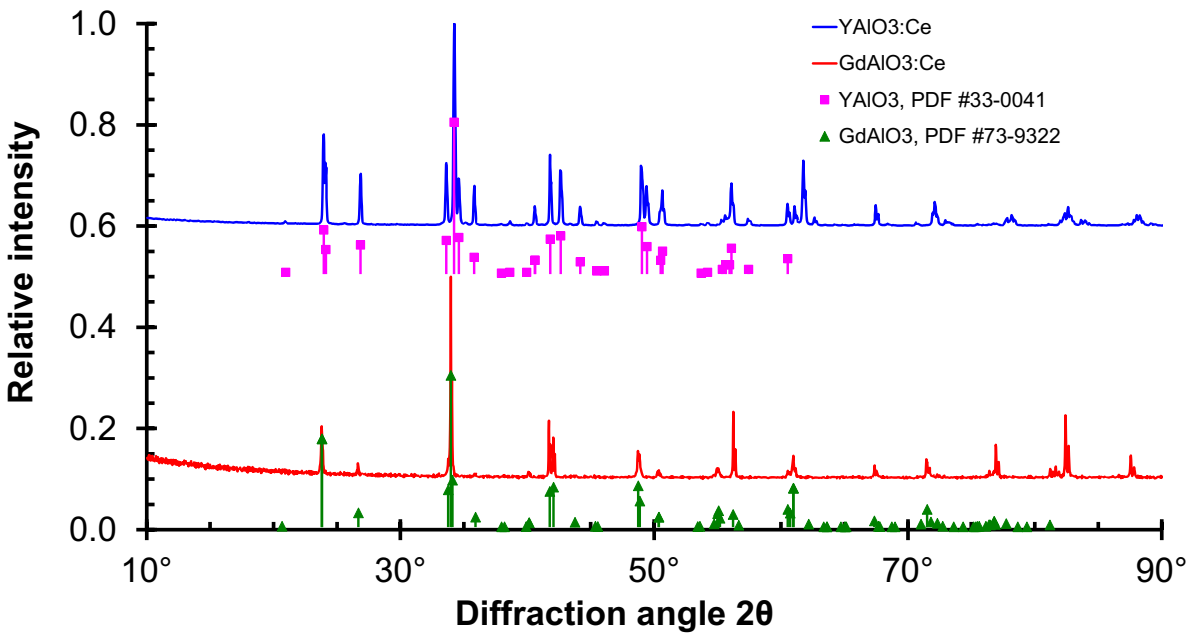

Figure S14: **Experimental structural characterization** X-ray diffraction patterns of the $YAlO_3$:Ce and $GdAlO_3$:Ce samples prepared by quenching of the melt, compared to the ICDD PDF-2 database records of the relevant phases.

4. Structural Analysis

The powder materials used to obtain consistent information about emission and excitation spectra of aluminate perovskites are phase-pure within detection limits of XRD and correspond perfectly to the respective database records of the intended phases.

References

[1] K. Momma and F. Izumi, Vesta 3 for three-dimensional visualization of crystal, volumetric and morphology data, Journal of applied crystallography **44**, 1272 (2011).

[2] J. P. Perdew, K. Burke, and M. Ernzerhof, Generalized gradient approximation made simple, Phys. Rev. Lett. **77**, 3865 (1996).

[3] D. Koller, F. Tran, and P. Blaha, Improving the modified Becke-Johnson exchange potential, Phys. Rev. B **85**, 155109 (2012).

[4] R. A. Jishi, O. B. Ta, and A. A. Sharif, Modeling of lead halide perovskites for photovoltaic applications, The Journal of Physical Chemistry C **118**, 28344 (2014).

[5] J. Sun, A. Ruzsinszky, and J. P. Perdew, Strongly constrained and appropriately normed semilocal density functional, Phys. Rev. Lett. **115**, 036402 (2015).

[6] V. Kolobanov, V. Mikhailin, N. Petrovnin, D. Spassky, and Y. Zorenko, Exciton creation in $LuAlO_3$ single crystalline film, physica status solidi (b) **243**, R60 (2006).

[7] A. Canning, A. Chaudhry, R. Boutchko, and N. Grønbech-Jensen, First-principles study of luminescence in Ce-doped inorganic scintillators, Phys. Rev. B **83**, 125115 (2011).

[8] V. I. Anisimov, J. Zaanen, and O. K. Andersen, Band theory and Mott insulators: Hubbard U instead of Stoner I, Phys. Rev. B **44**, 943 (1991).

[9] V. I. Anisimov, I. V. Solovyev, M. A. Korotin, M. T. Czyżyk, and G. A. Sawatzky, Density-functional theory and NiO photoemission spectra, Phys. Rev. B **48**, 16929 (1993).

[10] A. I. Liechtenstein, V. I. Anisimov, and J. Zaanen, Density-functional theory and strong interactions: Orbital ordering in Mott-Hubbard insulators, Phys. Rev. B **52**, R5467 (1995).

[11] P. Dorenbos and C. W. Van Eijk, *Proceedings of the international conference on inorganic scintillators and their applications, Delft, The Netherlands, 28 August-September 1, 1995: SCINT 95* (Delft University Press 1996).

[12] M. Buryi, V. Laguta, M. Nikl, V. Gorbenko, T. Zorenko, and Y. Zorenko, LPE growth and study of the Ce^{3+} incorporation in $LuAlO_3$:Ce single crystalline film scintillators, CrystEngComm **21**, 3313 (2019).

[13] D. N. Petrov and B. Angelov, Spin–orbit coupling and quasi–nephelauxetic effect in Ce^{3+}, Physica B: Condensed Matter **579**, 411912 (2020).